Colossal Room-Temperature Ferroelectric Polarizations in SrTiO₃/SrRuO₃ Superlattices Induced by Oxygen Vacancies

Jun Liang Lin,◇ Yuanwei Sun,◇ Ri He,◇ Yanxi Li, Zhicheng Zhong,* Peng Gao,* Xiang Zhao, Zhidong Zhang, and Zhan Jie Wang*

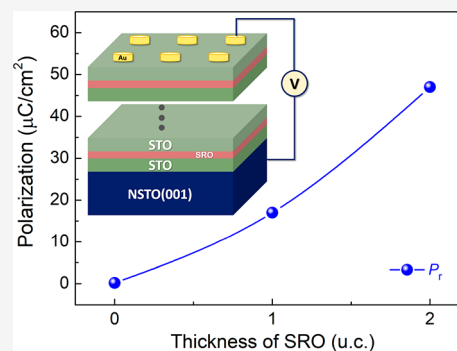Read Online

ACCESS | 📊 Metrics & More | 📖 Article Recommendations | 🆂🅸 Supporting Information

ABSTRACT: Artificial superlattices have demonstrated many unique phenomena not found in bulk materials. For this investigation, SrTiO₃/SrRuO₃ paraelectric/metallic superlattices with various stacking periods were synthesized via pulsed laser deposition. A robust room-temperature ferroelectric polarization (∼46 $\mu C/cm^2$) was found in the superlattices with 2 unit cell (u.c.) thick SrRuO₃ layers, despite the fact that neither SrTiO₃ nor SrRuO₃ is inherently ferroelectric. Results obtained from atomically resolved elemental mapping and X-ray photoelectron spectroscopy verified that oxygen vacancies accumulated at the SrTiO₃/SrRuO₃ interfaces, causing lattice distortions and increased tetragonality (c/a). The observed ferroelectric responses can be mainly attributed to the broken spatial inversion symmetry induced by the ordered distribution of oxygen vacancies at the SrTiO₃/SrRuO₃ interfaces, coupled with the triggering of external electric field. The resulting polarization mechanism induced by oxygen vacancies suggests viable ways for improving the electrical properties of ferroelectric materials, with the goal of expanding the functionality of a range of electronic devices.

KEYWORDS: *superlattices, SrTiO₃/SrRuO₃ interface, pulsed laser deposition, oxygen vacancy, ferroelectric polarization*

The complex transition metal oxide SrTiO₃ is a quantum paraelectric insulator with a perovskite-type ABO₃ structure;[1] importantly, its atomic positional fluctuations are able to suppress a ferroelectric transition. SrTiO₃ is also known as an incipient ferroelectric because the large electrical field can counteract the fluctuations and force the system into an ordered state, resulting in ferroelectricity at temperatures below 40 K.[2] At ultralow temperatures, SrTiO₃ is able to display ferroelectricity relatively easily, but the polarization intensity is typically less than 10 $\mu C/cm^2$.[3−6] Researchers continue to investigate the physical characteristics and mechanisms of SrTiO₃, and in particular its ferroelectric properties at room temperature. For instance, ferroelectricity in SrTiO₃ can be induced by strain effect,[7−9] A-site cation doping,[10] reducing oxygen pressure during deposition,[11] reducing dimensions,[12] and via optical excitation.[13] However, each of these approaches present distinct challenges in inducing a large ferroelectric polarization (less than 1.5 $\mu C/cm^2$) at room-temperature; moreover, it can be difficult to obtain essential macroscopic ferroelectric polarization data using ordinary ferroelectric testing instruments. Herein, we show that SrTiO₃/SrRuO₃ superlattices have robust ferroelectric polarization at room temperature. The remanent polarization is as high as 46 $\mu C/cm^2$, which is comparable to the typical Pb-based ferroelectric material Pb(Zr$_x$Ti$_{1-x}$)O₃.

In recent years SrTiO₃/SrRuO₃ superlattices have attracted significant attention due to their unique physical phenomena.
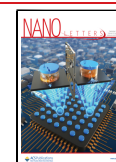
Of particular importance is that when the periodic thickness of each constituent material in the superlattice decreases, the synergy of size effect and interface effect may further optimize the functional properties of superlattice films. For example, it is known that the electron correlation effect can be affected by changing the periodic thickness of SrTiO₃ in SrTiO₃/SrRuO₃ superlattices, such that a previously unobserved 8-fold magnetic anisotropy was observed in magnetic SrRuO₃ monolayers.[14] Moreover, enhanced magnetoelectric properties,[15] magnetic ordering, and structural phase transitions,[16] as well as thermoelectric properties and spin-polarized two-dimensional electron gas[17,18] were also observed in SrTiO₃/SrRuO₃ superlattices. In each of these cited studies describing the various functional properties of SrTiO₃/SrRuO₃ superlattices, the role of SrRuO₃ was targeted. However, we believe that the structure and properties of SrTiO₃ may also play a role in the behavior of SrTiO₃/SrRuO₃ superlattices.

First-principles density functional theory (DFT) calculations indicate that by designing the oxygen vacancy formation energy profile and migration path across the oxide hetero-
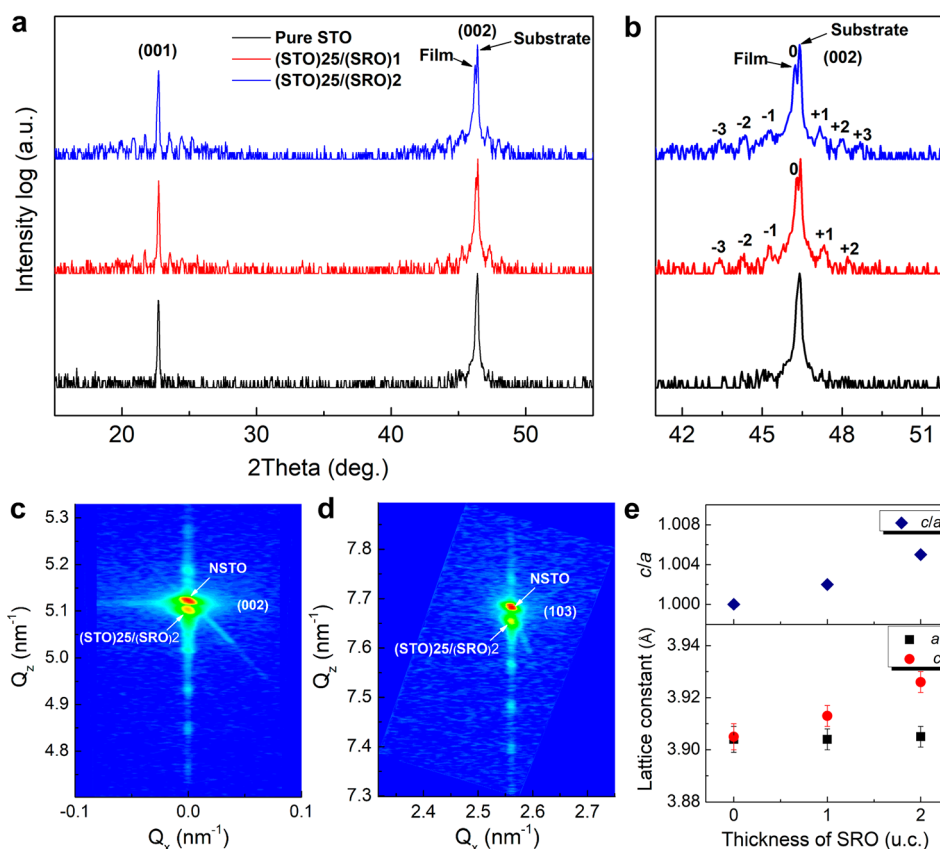
Figure 1. (a) HRXRD patterns of the STO film and the STO/SRO paraelectric/metallic superlattices with different SRO thicknesses and (b) enlarged HRXRD patterns around the (002) diffraction peaks. (c and d) RSM results for the (002) and (103) peaks of the STO_{25}/SRO_2 superlattice, respectively. (e) Calculated lattice parameters and the tetragonality (c/a) of the STO film and STO/SRO superlattices with different SRO thicknesses.

structure, the point defects can effectively break the inversion symmetry, thereby creating ferroelectricity in $SrTiO_3/SrRuO_3$ superlattices.[19] Nonetheless, confirmed experimental evidence for the presence of oxygen vacancies at the interfaces and the ability to measure macroscopic ferroelectric polarization are still lacking.

To study the ferroelectricity of $SrTiO_3/SrRuO_3$ superlattices, a key issue must be considered: the periodic thickness of $SrRuO_3$. Since $SrRuO_3$ is a metallic conductive oxide, the $SrTiO_3/SrRuO_3$ superlattice films may not show ferroelectricity due to the excessive leakage current. However, studies have shown that when the thickness of $SrRuO_3$ is less than 4 unit cells (u.c.), a metal−insulator transition will occur that greatly reduces conductivity.[20,21] In addition, a recent study report indicates that in $SrRuO_3/BaTiO_3$ superlattices, the coexistence of two-dimensional (2D) metallicity in the 1 u.c. thick $SrRuO_3$ layer, accompanied by the breaking of inversion symmetry, support electric polarization along the out-of-plane direction.[22] Therefore, in order to study the ferroelectricity of $SrTiO_3/SrRuO_3$ superlattices, one must adjust the periodic thickness of $SrRuO_3$ in the superlattice to no more than 3 u.c. Additionally, controlling the periodic thickness of $SrTiO_3$ to suppress the leakage current and maintain the possible long-range ferroelectric order is essential.

In this study, $SrTiO_3/SrRuO_3$ (STO/SRO) superlattices with various stacking periods were prepared via pulsed laser deposition (PLD). The periodic thicknesses of SRO and STO were controlled at 1−3 and 9−25 u.c., respectively. Figure 1a shows the $\theta-2\theta$ scan high-resolution X-ray diffraction

(HRXRD) patterns of the pure STO film and the STO/SRO superlattices with different stacking periods (25/1 and 25/2 u.c.) on NSTO (001) substrates. In all superlattice samples, only strong (00l) diffraction peaks are observed, indicating the highly preferred c-axis orientation of the films without an impurity phase. The epitaxial relationship between the superlattice films and the NSTO substrates featuring 4-fold symmetry was also confirmed by XRD phi scans of the {101} planes (Figure S1). As shown in Figure 1b, the main diffraction peaks of the superlattices do not overlap with the NSTO substrates, indicating the different lattice constants in the out-of-plane direction. The lattice constants of the STO/SRO superlattices were accurately measured utilizing reciprocal space mapping (RSM). For example, Figure 1c,d provides RSM results around the reflections of the (002) and (103) planes of the STO_{25}/SRO_2 superlattice, respectively. The RSM results for the pure STO film and the STO_{25}/SRO_1 superlattices are shown in Figure S2. Figure 1e shows the calculated lattice constants and tetragonality (c/a) of these samples. The out-of-plane lattice constant and the tetragonality of the superlattices increase with increasing SRO thickness. Typically, the tetragonality of STO in the pure film is close to 1; that is, pure STO film retains the symmetry of spatial inversion. However, in STO/SRO superlattices the tetragonality is greater than 1. For bulk materials, the increase of tetragonality does not mean the breaking of inversion symmetry, but for superlattice materials composed of a large number of heterogeneous interfaces, the increase of tetragonality caused by the accumulation of interface defects can be
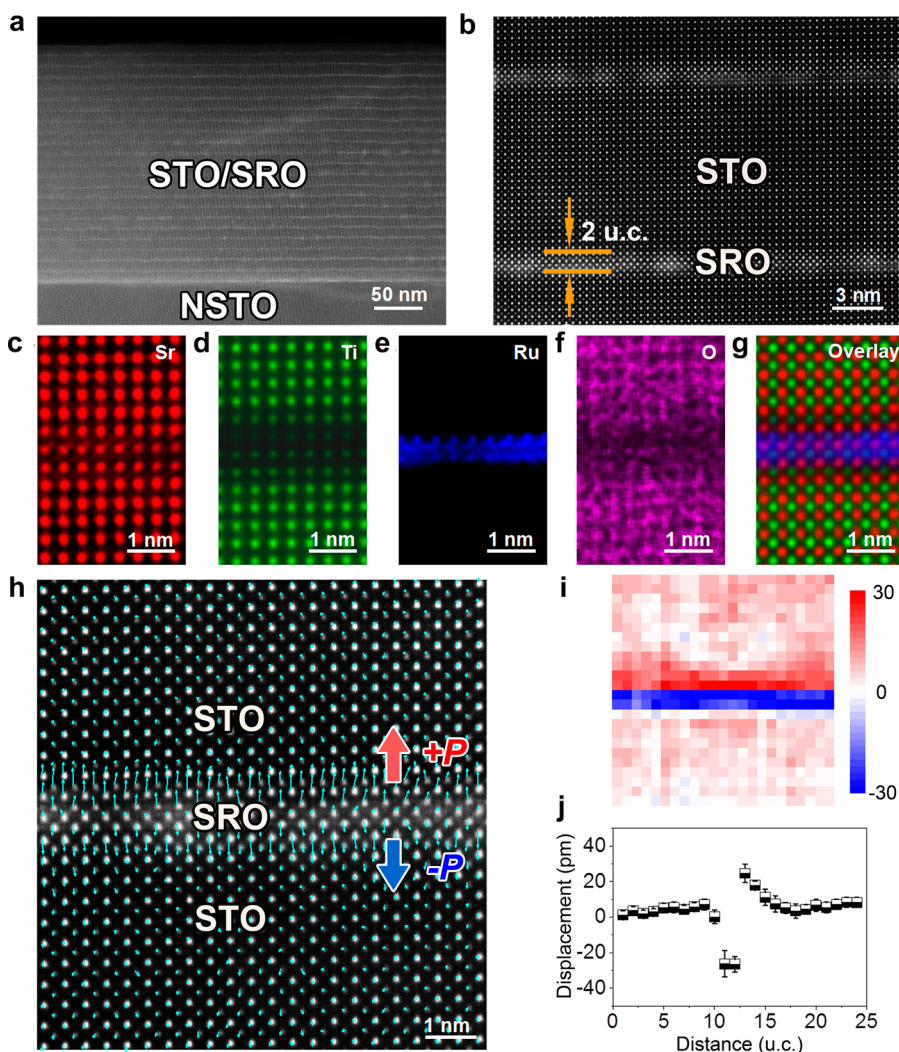
Figure 2. (a and b) Low- and high-magnification HAADF-STEM images of the STO_{25}/SRO_2 superlattice. (c−g) Atomically resolved EDS elemental mappings at the STO/SRO interface. (h) Atomically resolved HAADF-STEM image overlaid with the displacement vectors between Sr and Ti (Ru) columns at the STO/SRO interfaces. (i) Out-of-plane polar displacement map derived from (h). (j) Statistical results of the average displacements of (i); the error bar is the standard deviation.

considered as the breaking of spatial inversion symmetry. Our previous theoretical calculation work also show that the inversion symmetry can be compositionally broken by isolated oxygen vacancies, which is in strong contrast to the conservation of inversion symmetry in bulk crystals; thus, the symmetry of spatial inversion is broken.[19] Considering that the lattice parameter of STO is 3.905 Å and that of pseudocubic SRO is 3.923 Å, the maximum in-plane tensile strain of STO is only 0.46% in theory when the lattice parameters of STO and NSTO substrates are the same. According to theoretical calculations,[19] the lattice mismatch strain between STO and SRO is not sufficient to drive such a large increase in the tetragonality of the STO/SRO superlattice films, so it has little effect on polarization.

The microstructures of the STO/SRO superlattices were studied by aberration-corrected STEM. As shown in Figure 2a, for example, the low-magnification high-angle annular dark-field (HAADF) image indicates that an alternating periodic arrangement of STO and SRO layers had clearly formed in the STO_{25}/SRO_2 superlattice, with a total thickness of approximately 250 nm. Mapping data obtained via low-magnification energy-dispersive X-ray spectroscopy (EDS) (Figure S3)

clearly indicate the layered distribution of Ti and Ru within the STO/SRO superlattice. Furthermore, Sr atoms were found to be evenly distributed within the superlattice. Because the HAADF image with atomic-number-dependent contrast is quite insensitive to lighter oxygen atoms, the distribution of individual oxygen atoms cannot be observed as clearly as other atoms. From the chemical elemental mapping for oxygen atoms shown in Figures 2f and S3e, it can be seen that the black contrast layer representing the reduced concentration of oxygen atoms is around the SRO layer, indicating that oxygen vacancies accumulate at the STO/SRO interfaces. In addition to structural discontinuity,[23] the formation energy of oxygen vacancies at the STO/SRO heterointerfaces is relatively low (see Figure 5a) due to asymmetric bonding. The distribution of oxygen vacancies within the STO/SRO superlattices was also verified using X-ray photoelectron spectroscopy (XPS) results (Figure S4). The high-magnification HAADF image (Figure 2b) and corresponding atomic EDS elemental mapping results (Figure 2c−g) clearly show the oxygen-deficient interfacial structure within the STO/SRO superlattice; additionally, we are able to confirm that the thickness of the SRO layer is indeed 2 u.c..
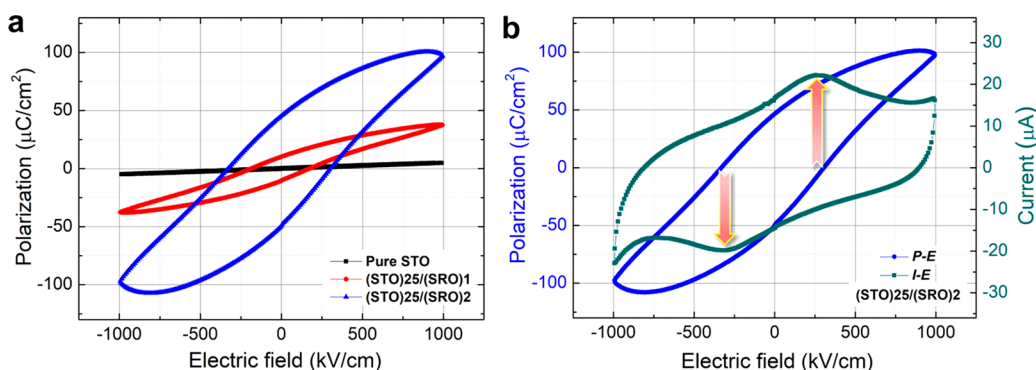
Figure 3. (a) $P-E$ hysteresis loops of the pure STO film and the STO_{25}/SRO_1 and the STO_{25}/SRO_2 superlattices. (b) $P-E$ hysteresis loop and $I-E$ curve of the STO_{25}/SRO_2 superlattice.

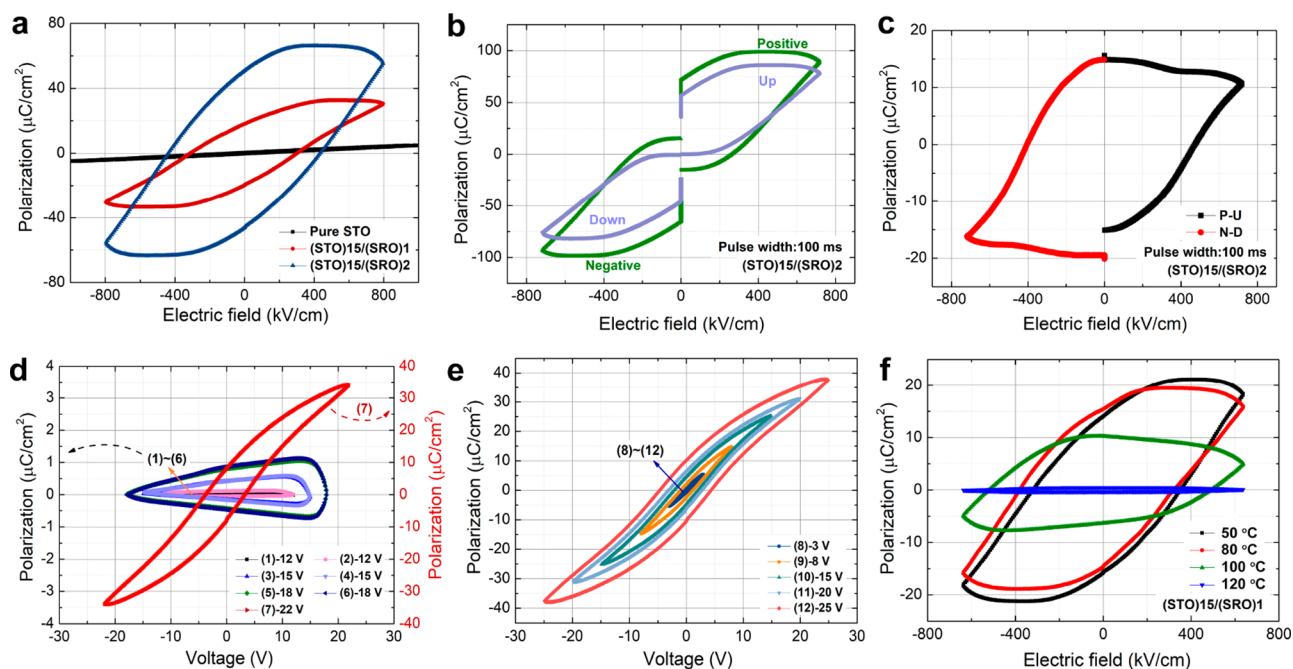**Figure 4.** (a) $P-E$ hysteresis loops of the pure STO film and the STO_{15}/SRO_1 and the STO_{15}/SRO_2 superlattices. (b) $P-E$ hysteresis loop of the STO_{15}/SRO_2 superlattice using a positive-up–negative-down (PUND) procedure under a triangular ac electric field with the pulse width of 100 ms. (c) The purely hysteresis component of the STO_{15}/SRO_2 superlattice obtained by subtracting the nonhysteresis contribution ("up" and "down" runs) from the total one ("positive" and "negative" runs). (d and e) $P-E$ hysteresis loops of the STO_{25}/SRO_1 superlattice during the repeatedly applied voltages from small to large voltages, and the measurement sequence is marked. (f) $P-E$ hysteresis loops of the STO_{15}/SRO_1 superlattice measured at different temperatures.

The details of the interfacial structure were further investigated by atomically resolved HAADF polar mapping (Figure 2h); results confirmed that the polar vectors were in opposing directions, indicating a tail-to-tail polarization configuration. The statistical results of the average displacements near the STO/SRO interface can be seen in Figure 2i,j. In the absence of an external electric field, such polar behavior will not cause polarization phenomenon at the macroscopic level. However, when an external electric field is applied, the polarization on one side of the SRO layer may be enhanced, while the polarization on the opposite side may be reversed; thus, polarization will be generated at the macroscopic level.

Figure 3a shows the $P-E$ hysteresis loops of the pure STO film and the STO/SRO superlattices with different stacking periods (25/1 and 25/2 u.c.) measured at room temperature. The pure STO film displays a nearly linear polarization response, which is consistent with its paraelectric properties.

By contrast, the superlattices exhibit a nonlinear polarization response (i.e., ferroelectric-like $P-E$ hysteresis loops). We also determined that the remanent polarization (P_r) increased with a concurrent increase in SRO thickness from 1 to 2 u.c. Moreover, the P_r of the STO/SRO superlattice with the 2 u.c. SRO layers reached 46 $\mu C/cm^2$, which is much larger than the measured room-temperature value obtained in strained $SrTiO_3$ films ($\sim$1.5 $\mu C/cm^2$).[6,11] Furthermore, when the SRO thickness was then increased to 3 u.c., the shape of the $P-E$ hysteresis loop clearly became abnormal (Figure S5), which we attribute to an increase in leakage current (Figure S6). As reported earlier, the electrical conductivity of SRO is known to increase with expanding SRO thickness from 1 to 3 u.c.,[21] leading to a decrease in the overall insulation of superlattices. Therefore, in order to obtain the STO/SRO superlattices with lower leakage current, the thickness of SRO layers should not exceed 2 u.c..
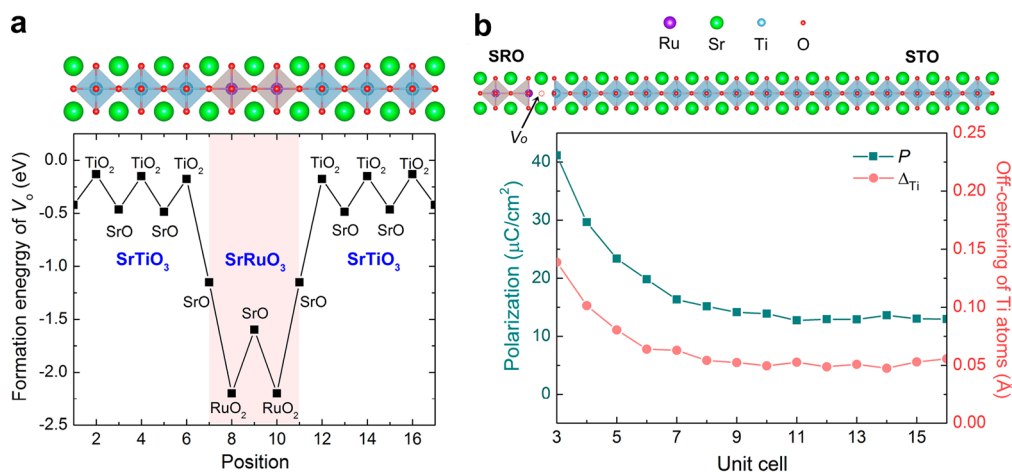
Figure 5. (a) Position dependence of the relative formation energy of an oxygen vacancy in a STO_{15}/SRO_2 superlattice. (b) Polarization and the off-centering displacement of Ti atoms from the center-of-mass of oxygen octahedra in the STO layer as a function of the position of the STO/SRO superlattice for the case with an oxygen vacancy at the SrO interface.

It should be noted that many artifacts are incorrectly thought to possess ferroelectric properties.[24] However, the appearance of the switching peaks in the $I-E$ curves of our STO/SRO superlattices (Figures 3b and S7) provides powerful evidence for the existence of true ferroelectricity. The switching field for the $I-E$ curve (288.09 kV/cm) and the $P-E$ curve (315.04 kV/cm) are basically the same; therefore, the position of the switching peaks in the $I-E$ curves corresponds to the coercive field in the $P-E$ hysteresis loop, implying the existence of ferroelectric polarization reversal.

We then reduced the thickness of the STO layer to study the effect of its thickness on the polarization properties of the superlattices. Figure 4a shows the $P-E$ hysteresis loops of the pure STO film and the STO_{15}/SRO_1 and STO_{15}/SRO_2 superlattices measured at room temperature. Compared with the 25 u.c. thick STO/SRO superlattices (Figure 3a), the superlattices with an STO thickness of 15 u.c. appeared to possess greater polarization intensity, but with the broad $P-E$ hysteresis loop shape. This finding could be attributed to a decrease in the thickness of the insulating STO in the superlattices, which will amplify the effect of leakage current on the $P-E$ hysteresis loops. To counter this effect, we incorporated the positive−up−negative−down (PUND) measurement method, which is able to distinguish the contribution of leakage current to polarization curve and represents a powerful method for capturing true ferroelectric behavior.[25,26] The applied voltage waveform for the PUND measurement is shown in Figure S8a, and the experimental results for the STO_{15}/SRO_2 superlattice are shown in Figure 4b. Figure 4c displays the purely hysteresis component of the STO_{15}/SRO_2 superlattice, which we obtained from the data presented in Figure 4b by subtracting the nonhysteresis contribution ("up" and "down" runs) from the total ("positive" and "negative" runs). The switched polarization of the STO_{15}/SRO_2 superlattice obtained via the PUND method was approximately 15 $\mu C/cm^2$, which indicates that the STO_{15}/SRO_2 superlattices do exhibit true ferroelectric behavior despite leakage current makes a major contribution to the polarization measured via conventional $P-E$ hysteresis measurements. We also confirmed that the switched polarization decreased with a decrease in the pulse width during application of PUND pulses (Figures S8b and S8c), suggesting that (a) a shorter pulse width is unable to trigger polarization reversal and (b) the oxygen-

vacancy-induced polarization mechanism in STO/SRO superlattices is different from that of traditional ferroelectric materials.

During the process of measuring the $P-E$ hysteresis loops, we noted that the occurrence of ferroelectric polarization necessitated the application of repeated voltage from low to high (Figure 4d,e); this feature indicates that there may be a polarization wake-up effect in the STO/SRO superlattices, similar to that found in yttrium-doped hafnium oxides.[27] For yttrium-doped hafnium oxides, the origin of ferroelectricity is typically associated with changes in crystal structure, which is caused by doping-induced artificial defects and the redistribution of oxygen vacancies under an applied electric field (wake-up effect). Similar to yttrium-doped hafnium oxides, the occurrence of the nonlinear polarization response in the STO/SRO superlattices can be attributed to the broken spatial inversion symmetry induced by oxygen vacancies, coupled with the triggering of an applied external electric field. However, the difference is that the oxygen vacancies are mainly distributed in the region of the STO/SRO interfaces. When the direction of the external electric field changes, however, oxygen vacancies may move to the upper and lower interfaces of the SRO layers to maintain the continuity of interlayer polarization and to achieve the switchable bidirectional polarization. In the work of Bark et al.,[28] a switchable polarization in a $LaAlO_3/SrTiO_3$ heterostructure was observed by piezoresponse force microscopy, which was also attributed to the motion of oxygen vacancies under an action of external electric field.

The effect of oxygen vacancies on ferroelectricity can also be verified by examining the temperature-dependence of ferroelectricity. As shown in Figure 4f, the $P-E$ hysteresis loop of the STO_{15}/SRO_1 superlattice became distorted when we increased the test temperature from 50 to 120 °C, at which point it became a straight line. As documented in the literature, oxygen vacancies can migrate easily with a rise in temperature.[27,29] For yttrium-doped hafnium oxides, increasing the temperature to 100 °C will accelerate the wake-up process. In contrast, for the STO/SRO superlattices the orderly distribution of oxygen vacancies at the STO/SRO interfaces will become disordered at elevated temperatures, which will lead to the loss of ferroelectricity in these superlattices.

Utilizing first-principles DFT calculations, we also investigated why oxygen vacancies were found to be segregated at

the STO/SRO interfaces, as well as the effects of oxygen vacancies on the ferroelectricity of STO/SRO superlattices. To do so, we inspected the energetically favored locations of oxygen vacancies by comparing the relative formation energies of oxygen vacancy (E^{Vo}) in the $(STO)_{15}/(SRO)_2$ superlattices. Figure 5a shows the E^{Vo} near the STO/SRO interface of the $(STO)_{15}/(SRO)_2$ supercell, indicating that the E^{Vo} of the interfacial SrO layer is clearly smaller than that in the STO region, but larger than the one in the SRO region. However, according to DFT LDA + U calculations[30] and known experimental results,[31,32] oxygen diffusion in SRO is more difficult compared to that in STO, since the diffusion barrier of oxygen vacancy in bulk SRO is much higher (∼0.9 eV) than that of its STO analog (∼0.6 eV). As a result, the oxygen vacancy tends to segregate in SRO due to its lower formation energy; it then stops at two symmetrically interfacial SrO layers due to the high diffusion barrier in SRO. These calculation results are consistent with the orderly distribution of oxygen vacancies at the STO/SRO interfaces observed in our experiment (Figure 2).

In the $(STO)_{15}/(SRO)_2$ superlattice lacking oxygen vacancies, the calculation results showed a zero polarization at the interface. However, when an oxygen vacancy was introduced into the interfacial SrO layer, Ru atoms moved toward the defective interface, while Ti atoms moved away from the defective interface (see Figure 5b). The displacement of these atoms ranged from 0.05–0.13 Å, which is comparable to the conventional perovskite ferroelectrics.[33] As a result, the polar displacements of Ti atoms can induce long-range polarization in STO_{15}/SRO_2 superlattice with an oxygen vacancy at the SrO layer, as shown in Figure 5b. The long-range polarization in each unit cell of STO resulted in an average macroscopic polarization of 17.97 $\mu C/cm^2$ in the superlattice, which is consistent with experimental results obtained via using the PUND method (Figure 4c). When oxygen vacancies are introduced into the perovskite oxide heterostructure, band alignment and charge transfer may happen at the interface, so the insulating oxide may undergo an insulator–metal transition and become conductive, which is in conflict with ferroelectricity.[34,35] To identify the band alignment and charge transfer of the oxygen-deficient STO/SRO heterostructure, we calculated the layer-resolved partial density of states (PDOS) projected on the oxygen p and Ti/Ru d states, as shown in Figure S9, and we can confirm that the STO/SRO superlattice as a whole is in an insulating state (see the Supporting Information for the detailed discussion). Moreover, it must be mentioned that the defect-induced polarization is under a metastable state because of the locally distributed oxygen vacancies at the interfaces. Under experimental conditions, an abrupt change in applied voltage or frequency will result in the distortion of the hysteresis loop shape or the loss of polarization. To reduce leakage current and obtain optimal ferroelectric polarization, further research is needed to adjust the ratio of SRO to STO in STO/SRO superlattices.

To summarize, $SrTiO_3/SrRuO_3$ (STO/SRO) paraelectric/metallic superlattices with different stacking periods were prepared by PLD. Robust room-temperature ferroelectric polarizations were observed in the STO/SRO superlattices, despite the fact that neither STO nor SRO is inherently ferroelectric. This finding indicates that the ferroelectric response of these materials can be principally attributed to the broken spatial inversion symmetry induced by the orderly distribution of oxygen vacancies at the STO/SRO interfaces, coupled with the triggering of an applied external electric field. In addition, we propose that the polarization mechanism induced by oxygen vacancies will afford opportunities to enhance the electrical properties of ferroelectric materials and expand the functional range of device applications.

■ ASSOCIATED CONTENT

ⓢ Supporting Information

The Supporting Information is available free of charge at https://pubs.acs.org/doi/10.1021/acs.nanolett.2c02175.

> Details on sample preparations, characterization, and first-principles calculations; epitaxial relationship between the films and the substrates; RSM results of the pure STO film and the STO_{25}/SRO_1 superlattice; low-magnification EDS mapping results; Ti 2p and O 1s XPS spectra across the STO/SRO interface; $P-E$ hysteresis loop of the STO_{25}/SRO_3 superlattice; leakage current results; appearance of the switching peaks in the $I-E$ curve; PUND voltage waveform and the results for the pulse width of 5 ms (PDF)

■ AUTHOR INFORMATION

Corresponding Authors

Zhicheng Zhong − *Key Laboratory of Magnetic Materials and Devices, Zhejiang Province Key Laboratory of Magnetic Materials and Application Technology, Ningbo Institute of Materials Technology and Engineering, Chinese Academy of Sciences, Ningbo 315201, China; China Center of Materials Science and Optoelectronics Engineering, University of Chinese Academy of Sciences, Beijing 100049, China;* ⓞ orcid.org/0000-0003-1507-4814; Email: zhong@nimte.ac.cn

Peng Gao − *International Center for Quantum Materials, and Electron Microscopy Laboratory, School of Physics, Peking University, Beijing 100871, China; Collaborative Innovation Center of Quantum Matter, Beijing 100871, China;* ⓞ orcid.org/0000-0003-0860-5525; Email: p-gao@pku.edu.cn

Zhan Jie Wang − *School of Materials Science and Engineering, Shenyang University of Technology, Shenyang 110870, China;* ⓞ orcid.org/0000-0002-9288-4928; Email: wangzj@imr.ac.cn

Authors

Jun Liang Lin − *School of Materials Science and Engineering, Northeastern University, Shenyang 110819, China; Shenyang National Laboratory for Materials Science, Institute of Metal Research (IMR), Chinese Academy of Sciences (CAS), Shenyang 110016, China; College of Light Industry, Liaoning University, Shenyang 110036, China*

Yuanwei Sun − *International Center for Quantum Materials, and Electron Microscopy Laboratory, School of Physics, Peking University, Beijing 100871, China*

Ri He − *Key Laboratory of Magnetic Materials and Devices, Zhejiang Province Key Laboratory of Magnetic Materials and Application Technology, Ningbo Institute of Materials Technology and Engineering, Chinese Academy of Sciences, Ningbo 315201, China*

Yanxi Li − *Department of Materials Science and Engineering, Stanford University, Stanford, California 94305, United States*

Xiang Zhao − *School of Materials Science and Engineering, Northeastern University, Shenyang 110819, China*

Zhidong Zhang − *Shenyang National Laboratory for Materials Science, Institute of Metal Research (IMR), Chinese Academy of Sciences (CAS), Shenyang 110016, China;* 🄾 orcid.org/0000-0002-6203-0171

Complete contact information is available at:
https://pubs.acs.org/10.1021/acs.nanolett.2c02175

Author Contributions

◇J.L.L., Y.S., and R.H. contributed equally to this work. The manuscript was written through contributions of all authors. All authors have given approval to the final version of the manuscript.

Notes

The authors declare no competing financial interest.

■ REFERENCES

(1) Müller, K. A.; Burkard, H. SrTiO$_3$: An intrinsic quantum paraelectric below 4 K. *Phys. Rev. B* **1979**, *19* (7), 3593−3602.

(2) Hemberger, J.; Lunkenheimer, P.; Viana, R.; Bohmer, R.; Loidl, A. Electric-field-dependent dielectric constant and nonlinear susceptibility in SrTiO$_3$. *Phys. Rev. B* **1995**, *52* (18), 13159−13162.

(3) Ang, C.; Yu, Z.; Vilarinho, P.; Baptista, J. Bi: SrTiO$_3$: A quantum ferroelectric and a relaxor. *Phys. Rev. B* **1998**, *57* (13), 7403.

(4) Itoh, M.; Wang, R.; Inaguma, Y.; Yamaguchi, T.; Shan, Y.; Nakamura, T. Ferroelectricity induced by oxygen isotope exchange in strontium titanate perovskite. *Phys. Rev. Lett.* **1999**, *82* (17), 3540.

(5) Zubko, P.; Catalan, G.; Buckley, A.; Welche, P. R.; Scott, J. F. Strain-gradient-induced polarization in SrTiO$_3$ single crystals. *Phys. Rev. Lett.* **2007**, *99* (16), 167601.

(6) Jang, H. W.; Kumar, A.; Denev, S.; Biegalski, M. D.; Maksymovych, P.; Bark, C. W.; Nelson, C. T.; Folkman, C. M.; Baek, S. H.; Balke, N.; Brooks, C. M.; Tenne, D. A.; Schlom, D. G.; Chen, L. Q.; Pan, X. Q.; Kalinin, S. V.; Gopalan, V.; Eom, C. B. Ferroelectricity in strain-free SrTiO$_3$ thin films. *Phys. Rev. Lett.* **2010**, *104* (19), 197601.

(7) Warusawithana, M. P.; Cen, C.; Sleasman, C. R.; Woicik, J. C.; Li, Y.; Kourkoutis, L. F.; Klug, J. A.; Li, H.; Ryan, P.; Wang, L.-P.; et al. A ferroelectric oxide made directly on silicon. *Science* **2009**, *324* (5925), 367−370.

(8) Haeni, J.; Irvin, P.; Chang, W.; Uecker, R.; Reiche, P.; Li, Y.; Choudhury, S.; Tian, W.; Hawley, M.; Craigo, B.; et al. Room-temperature ferroelectricity in strained SrTiO$_3$. *Nature* **2004**, *430* (7001), 758.

(9) Xu, R.; Huang, J.; Barnard, E. S.; Hong, S. S.; Singh, P.; Wong, E. K.; Jansen, T.; Harbola, V.; Xiao, J.; Wang, B. Y.; et al. Strain-induced room-temperature ferroelectricity in SrTiO$_3$ membranes. *Nat. Commun.* **2020**, *11* (1), 3141.

(10) Durán, A.; Martínez, E.; Díaz, J. A.; Siqueiros, J. M. Ferroelectricity at room temperature in Pr-doped SrTiO$_3$. *J. Appl. Phys.* **2005**, *97* (10), 104109.

(11) Kim, Y. S.; Kim, D. J.; Kim, T. H.; Noh, T. W.; Choi, J. S.; Park, B. H.; Yoon, J. G. Observation of room-temperature ferroelectricity in tetragonal strontium titanate thin films on SrTiO$_3$ (001) substrates. *Appl. Phys. Lett.* **2007**, *91* (4), 042908.

(12) Lee, D.; Lu, H.; Gu, Y.; Choi, S. Y.; Li, S. D.; Ryu, S.; Paudel, T. R.; Song, K.; Mikheev, E.; Lee, S.; Stemmer, S.; Tenne, D. A.; Oh, S. H.; Tsymbal, E. Y.; Wu, X.; Chen, L. Q.; Gruverman, A.; Eom, C. B. Emergence of room-temperature ferroelectricity at reduced dimensions. *Science* **2015**, *349* (6254), 1314−7.

(13) Nova, T. F.; Disa, A. S.; Fechner, M.; Cavalleri, A. Metastable ferroelectricity in optically strained SrTiO$_3$. *Science* **2019**, *364* (6445), 1075−1079.

(14) Cui, Z.; Grutter, A. J.; Zhou, H.; Cao, H.; Dong, Y.; Gilbert, D. A.; Wang, J.; Liu, Y. S.; Ma, J.; Hu, Z.; et al. Correlation-driven eightfold magnetic anisotropy in a two-dimensional oxide monolayer. *Sci. Adv.* **2020**, *6* (15), eaay0114.

(15) Jeong, S. G.; Han, G.; Song, S.; Min, T.; Mohamed, A. Y.; Park, S.; Lee, J.; Jeong, H. Y.; Kim, Y. M.; Cho, D. Y.; Choi, W. S. Propagation control of octahedral tilt in SrRuO$_3$ via artificial heterostructuring. *Adv. Sci.* **2020**, *7*, 2001643.

(16) Gu, M.; Xie, Q.; Shen, X.; Xie, R.; Wang, J.; Tang, G.; Wu, D.; Zhang, G. P.; Wu, X. S. Magnetic ordering and structural phase transitions in a strained ultrathin SrRuO$_3$/SrTiO$_3$ superlattice. *Phys. Rev. Lett.* **2012**, *109* (15), 157003.

(17) García-Fernández, P.; Verissimo-Alves, M.; Bilc, D. I.; Ghosez, P.; Junquera, J. First-principles modeling of the thermoelectric properties of SrTiO$_3$/SrRuO$_3$ superlattices. *Phys. Rev. B* **2012**, *86* (8), 085305.

(18) Verissimo-Alves, M.; Garcia-Fernandez, P.; Bilc, D. I.; Ghosez, P.; Junquera, J. Highly confined spin-polarized two-dimensional electron gas in SrTiO$_3$/SrRuO$_3$ superlattices. *Phys. Rev. Lett.* **2012**, *108* (10), 107003.

(19) He, R.; Lin, J. L.; Liu, Q.; Liao, Z.; Shui, L.; Wang, Z. J.; Zhong, Z.; Li, R. W. Emergent ferroelectricity in otherwise nonferroelectric oxides by oxygen vacancy design at heterointerfaces. *ACS Appl. Mater. Interfaces* **2020**, *12* (40), 45602−45610.

(20) Chang, Y. J.; Kim, C. H.; Phark, S. H.; Kim, Y. S.; Yu, J.; Noh, T. W. Fundamental thickness limit of itinerant ferromagnetic SrRuO$_3$ thin films. *Phys. Rev. Lett.* **2009**, *103* (5), 057201.

(21) Xia, J.; Siemons, W.; Koster, G.; Beasley, M. R.; Kapitulnik, A. Critical thickness for itinerant ferromagnetism in ultrathin films of SrRuO$_3$. *Phys. Rev. B* **2009**, *79* (14), 140407R.

(22) Ye, M.; Hu, S.; Zhu, Y.; Zhang, Y.; Ke, S.; Xie, L.; Zhang, Y.; Hu, S.; Zhang, D.; Luo, Z.; Gu, M.; He, J.; Zhang, P.; Zhang, W.; Chen, L. Electric polarization switching on an atomically thin metallic oxide. *Nano Lett.* **2021**, *21* (1), 144−150.

(23) He, B.; Wang, Z. Enhancement of the electrical properties in BaTiO$_3$/PbZr$_{0.52}$Ti$_{0.48}$O$_3$ ferroelectric superlattices. *ACS Appl. Mater. Interfaces* **2016**, *8* (10), 6736−42.

(24) Scott, J. F. Ferroelectrics go bananas. *J-Phys-Condens. Mater.* **2008**, *20* (2), 021001.

(25) Horiuchi, S.; Kumai, R.; Tokura, Y. Hydrogen-bonding molecular chains for high-temperature ferroelectricity. *Adv. Mater.* **2011**, *23* (18), 2098−2103.

(26) Chai, Y.; Oh, Y. S.; Wang, L.; Manivannan, N.; Feng, S.; Yang, Y.; Yan, L.; Jin, C.; Kim, K. H. Intrinsic ferroelectric polarization of orthorhombic manganites with *E*-type spin order. *Phys. Rev. B* **2012**, *85* (18), 184406.

(27) Starschich, S.; Menzel, S.; Böttger, U. Evidence for oxygen vacancies movement during wake-up in ferroelectric hafnium oxide. *Appl. Phys. Lett.* **2016**, *108* (3), 032903.

(28) Bark, C. W.; Sharma, P.; Wang, Y.; Baek, S. H.; Lee, S.; Ryu, S.; Folkman, C. M.; Paudel, T. R.; Kumar, A.; Kalinin, S. V.; Sokolov, A.; Tsymbal, E. Y.; Rzchowski, M. S.; Gruverman, A.; Eom, C. B. Switchable induced polarization in LaAlO$_3$/SrTiO$_3$ heterostructures. *Nano Lett.* **2012**, *12* (4), 1765−71.

(29) Lin, D.; Kwok, K. W.; Chan, H. L. W. Double hysteresis loop in Cu-doped K$_{0.5}$Na$_{0.5}$NbO$_3$ lead-free piezoelectric ceramics. *Appl. Phys. Lett.* **2007**, *90* (23), 232903.

(30) Cuong, D. D.; Lee, B.; Choi, K. M.; Ahn, H.-S.; Han, S.; Lee, J. Oxygen vacancy clustering and electron localization in oxygen-deficient $SrTiO_3$: LDA + U study. *Phys. Rev. Lett.* **2007**, *98* (11), 115503.

(31) Schraknepper, H.; Baumer, C.; Dittmann, R.; De Souza, R. A. Complex behaviour of vacancy point-defects in $SrRuO_3$ thin films. *Phys. Chem. Chem. Phys.* **2015**, *17* (2), 1060−9.

(32) De Souza, R. A.; Metlenko, V.; Park, D.; Weirich, T. E. Behavior of oxygen vacancies in single-crystal $SrTiO_3$: equilibrium distribution and diffusion kinetics. *Phys. Rev. B* **2012**, *85* (17), 174109.

(33) Takenaka, H.; Grinberg, I.; Shin, Y.-H.; Rappe, A. M. Computational studies of lead-based relaxor ferroelectrics. *Ferroelectrics* **2014**, *469* (1), 1−13.

(34) Zhong, Z.; Hansmann, P. Band alignment and charge transfer in complex oxide interfaces. *Phys. Rev. X* **2017**, *7* (1), 011023.

(35) He, R.; Jiang, P.; Lu, Y.; Song, Y.; Chen, M.; Jin, M.; Shui, L.; Zhong, Z. Polarity-induced electronic and atomic reconstruction at $NdNiO_2/SrTiO_3$ interfaces. *Phys. Rev. B* **2020**, *102* (3), 035118.